EXPRESS LETTER

Depth profiles of resistivity and spectral IP for active modern submarine hydrothermal deposits: a case study from the Iheya North Knoll and the Iheya Minor Ridge in Okinawa Trough, Japan

Shogo Komori[1][*] [iD], Yuka Masaki[2], Wataru Tanikawa[3], Junji Torimoto[2], Yusuke Ohta[4], Masato Makio[5], Lena Maeda[6], Jun-ichiro Ishibashi[7], Tatsuo Nozaki[2], Osamu Tadai[8] and Hidenori Kumagai[2]

Abstract

Submarine hydrothermal deposits are one of the promising seafloor mineral resources, because they can store a large amount of metallic minerals as sulfides. The present study focuses on the electrical properties of active modern submarine hydrothermal deposits, in order to provide constraints on the interpretation of electrical structures obtained from marine electromagnetic surveys. Measurements of resistivity and spectral induced polarization (IP) were made using drillcore samples taken from the Iheya North Knoll and the Iheya Minor Ridge in Okinawa Trough, Japan. These hydrothermal sediments are dominantly composed of disseminated sulfides, with minor amounts of massive sulfide rocks. The depth profiles of resistivity and spectral IP properties were successfully revealed to correspond well to layer-by-layer lithological features. Comparison with other physical properties and occurrence of constituent minerals showed that resistivity is essentially sensitive to the connectivity of interstitial fluids, rather than by sulfide and clay content. This suggests that, in active modern submarine hydrothermal systems, not only typical massive sulfide rocks but also high-temperature hydrothermal fluids could be imaged as low-resistivity anomalies in seabed surveys. The spectral IP signature was shown to be sensitive to the presence or absence of sulfide minerals, and total chargeability is positively correlated with sulfide mineral abundance. In addition, the massive sulfide rock exhibits the distinctive IP feature that the phase steadily increases with a decrease of frequency. These results show the effective usage of IP for developing and improving marine IP exploration techniques.

Keywords: Submarine hydrothermal deposit, Sulfide mineral, Resistivity, Induced polarization (IP), Iheya North Knoll, Iheya Minor Ridge

Introduction

Exploration and exploitation of submarine hydrothermal deposits in Japan is becoming increasingly important for the steady supply of metal resources to Japanese industry. Metallic elements such as iron, copper, lead, and zinc are usually included in these deposits as sulfide minerals,

such as pyrite, chalcopyrite, galena, and sphalerite, respectively. It is well known that most sulfide minerals, except for sphalerite, exhibit an anomalous signature of the induced polarization (IP) effect (e.g., Pelton et al. 1978). Revil et al. (2015a, b) investigated complex electrical properties of disseminated sulfides with a wide range of frequencies of alternating current (AC) and provided the most recent theory of the IP effect based on semi-conduction mechanism (migration of hole and electron) inside the sulfide particles. The investigators showed that

*Correspondence: komori.shogo@aist.go.jp
[1] Geological Survey of Japan (GSJ), AIST, Central 7, Higashi 1-1-1, Tsukuba, Ibaraki, Japan
Full list of author information is available at the end of the article

Komori *et al. Earth, Planets and Space* (2017) 69:114

Page 2 of 10

the IP effect makes the sulfide particles very conductive at high frequencies and perfectly insulating at low frequencies. In general, electromagnetic investigations are believed to be effective in finding submarine sulfide deposits and have been conducted in order to reveal conductive anomalies related to the presence of deposits (e.g., Kowalczyk 2008; Okada et al. 2017). However, the IP effect makes it possible for sulfide-bearing sediments to be both conductive and insulating, depending on the frequency of the current. Therefore, understanding of the IP effect of rock and sediment samples taken from submarine hydrothermal deposits is crucial for reducing uncertainties in interpretations of geophysical structure.

The present study measured the electrical properties of drillcore samples taken from Iheya North Knoll and the Iheya Minor Ridge, the active modern submarine hydrothermal systems in Okinawa Trough, Japan. The resistivity and IP signature obtained were compared to other physical, lithological, and material data, in order to examine their controlling factors.

Site description

At Iheya North Knoll, numbers of research cruise discovered active hydrothermal areas, represented by Original, Natsu, and Aki Sites, for instance, as acoustic water column anomalies (Fig. 1a; Kasaya et al. 2015). A relatively new hydrothermal site was found at the southern flank of Iheya Minor Ridge, approximately 30 km south of the Iheya North Knoll (Chiba et al. 2014). During the CK16-01 Cruise (Expedition 908) using D/V Chikyu from February 11 to March 17, 2016, scientific drilling research was conducted at both sites [see CHIKYU 908 Cruise Data (http://www.godac.jamstec.go.jp/darwin/cruise/chikyu/908/e)]. At these sites, numbers of hydrothermal vents discharging black and white smokers are identified by seabed surveys using a remotely operated vehicle (ROV) prior to the drilling operation. Previous drilling programs [IODP Exp. 331 and CK14-04 Cruise (Exp. 907)] and seabed surveys have described the widely distributed hydrothermal area in the Iheya North Knoll (Takai et al. 2012, 2015). During the CK16-01 Cruise, eight sites were drilled and coring was performed at four of these (Fig. 1a; C9017, C9019, C9021, and C9023). Sites C9017 and C9019 are located at depths of approximately 1600 m water depth (WD) at the Iheya Minor Ridge, whereas sites C9021 and C9023 are at approximately 1000–1100 m WD at the Iheya North Knoll, respectively. Site-specific lithological features are described below, and detailed visual core descriptions are given in the cruise report (Kumagai et al. in prep.).

Site C9017

Site C9017 at Iheya Minor Ridge is a flat mound area with some active hydrothermal vents. Unaltered fresh basalt composes the uppermost unit (0–10 mbsf). Vesicles in this basalt are often filled with sulfides. The lower units (10–105 mbsf) consist of hydrothermal sediments with a variety of grain sizes and clay mineral components. Fine-grained pyrite is disseminated throughout the sediment, contributing to its blackish color. Relatively coarse-grained pyrrhotite, with an average diameter of approximately 1 mm, is present only at a depth of ca.70 mbsf (Fig. 1b).

Site C9021

Site C9021 is located between the Natsu and Aki Sites of Iheya North Knoll. Its seabed surface is mainly composed of unaltered pumice with soft hemipelagic sediment. The upper unit (0–67 mbsf), composed of unaltered to weakly altered pumiceous gravel (Fig. 1c), overlies a lower unit (67–98 mbsf) of altered and silicified volcanic rock. Sulfide mineral is negligibly present in the whitish matrices that are found almost entirely throughout the deeper unit, corresponding to the relatively small semiquantitative sulfide contents; some of the altered volcanic rocks in the lower unit are partly silicified.
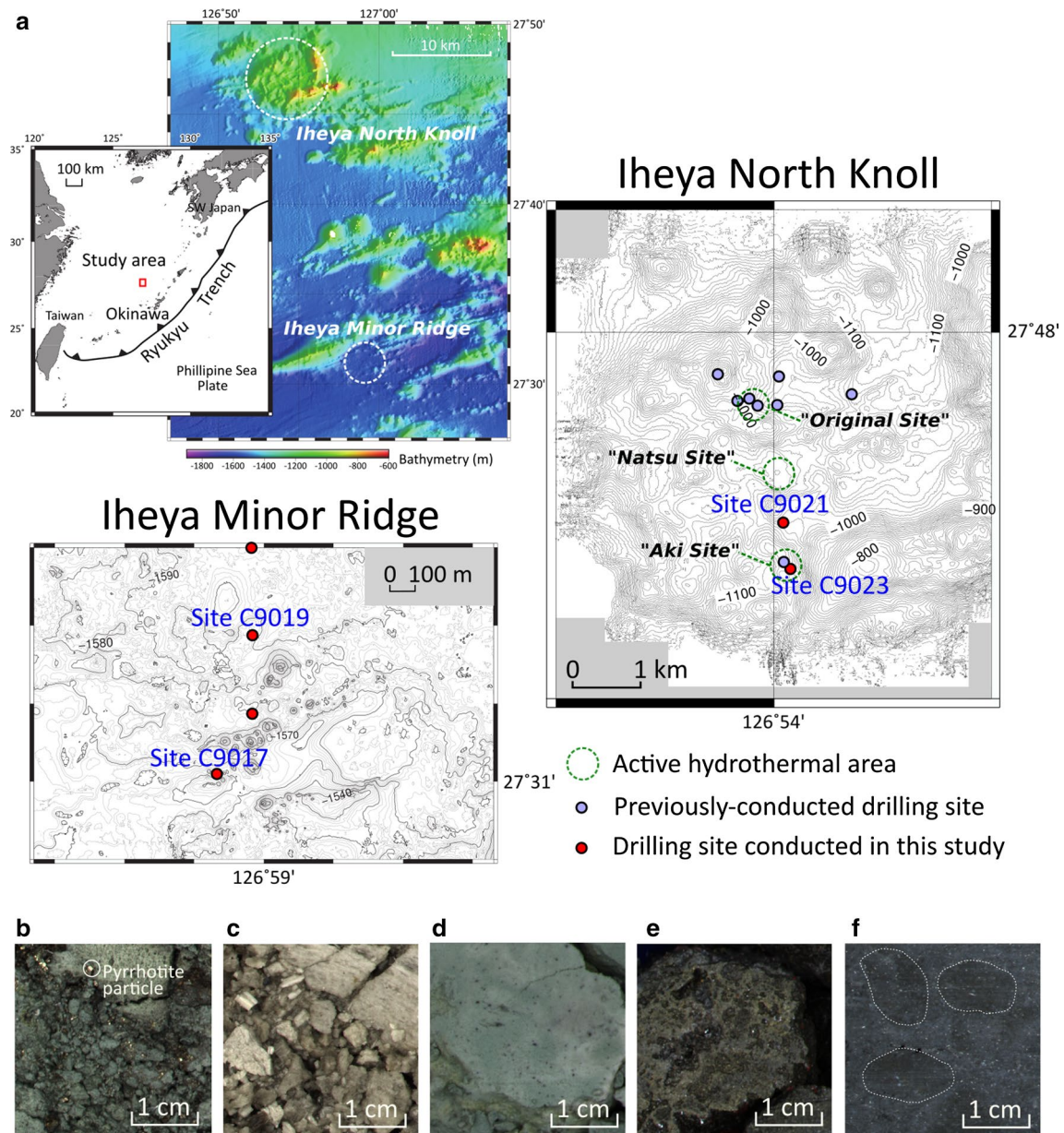
Site C9023

Site C9023 is located at the active hydrothermal mound of the Aki Site, Iheya North Knoll. At this site, the upper blackish hydrothermal sediments (0–79 mbsf) overlie greyish silicified volcanic rock (79–200 mbsf, Fig. 1d). Fine-grained sulfide mineral is disseminated, and pyrite, chalcopyrite, sphalerite, and galena are identified in the upper unit. In particular, massive sulfide rocks dominated by sulfide minerals are present only in the uppermost part of the upper unit (Fig. 1e). Based on the visual core description, the mode of occurrence of sulfide minerals seems to decrease with depth.

Methods

Promptly performed resistivity and IP properties measurements

The resistivity and IP properties of the drillcore samples were investigated immediately after drilling, in order to minimize water loss and oxidation of samples. The VersaSTAT4 impedance analyzer, manufactured by AMETEK, was used for complex resistivity measurements in the four-electrode configuration. Measurements on soft sediments were made by two copper wires (for current injection) and two non-polarizable Ag–AgCl electrodes (for potential measurement), while those on consolidated rocks were made by coupling the samples to non-polarizable $Cu–CuSO_4$ electrodes (Fig. 2). Prior to resistivity measurements on half-rounded shapes, calibration was performed to take into account the influence of the geometry on the observed data, by using NaCl solution

Komori *et al. Earth, Planets and Space* (2017) 69:114

Page 3 of 10

Fig. 1 **a** Location of Iheya North Knoll and Iheya Minor Ridge. **b** Site C9017 sample from a depth of 70.5 mbsf. Large particles of pyrrhotite are visible. **c** Site C9021 pumice sample from a depth of 21.6 mbsf. **d** Site C9023 silicified sample from a depth of 172.6 mbsf. **e** Site C9023 sample from a depth of 0 mbsf. It consists of massive sulfide rock. **f** Site C9017 sample from a depth of 34.4 mbsf. *White-dotted circles* represent patchy mottled textures rich in fine-grained sulfides

with known resistivities. In order to obtain spectral IP properties of the samples, we used an injection current with a wide range of frequencies between 0.01 Hz and 100 kHz. IP data with frequencies of 0.1 Hz–10 kHz were used for the analyses described below, in order to maintain a high signal-to-noise (S/N) ratio and to avoid additional Maxwell–Wagner effects in the high-frequency range (e.g., Leroy et al. 2008). All measurements were made at room temperature (~20 °C).

IP parameter estimation

The obtained spectral IP data were used to estimate IP parameters (DC resistivity, chargeability, Cole–Cole exponent, and time constant). In the present study, the

Komori *et al. Earth, Planets and Space* (2017) 69:114

Page 4 of 10
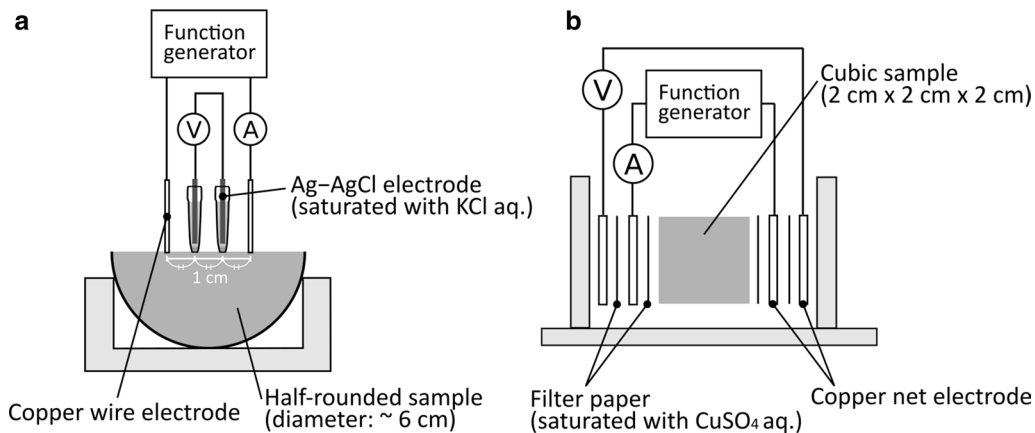
Fig. 2 Schematic configuration of resistivity and IP measurements for **a** unconsolidated sediments and **b** consolidated rocks

classical and basic Cole–Cole models (Pelton 1977) were adapted for IP data analyses as shown by:

$$\rho(\omega) = \rho_0 \left[1 - m \left(1 - \frac{1}{1 + (i\omega\tau)^c} \right) \right], \tag{1}$$

where $\rho(\omega)$ is the frequency-dependent complex resistivity, ρ_0 is the DC resistivity, ω is the frequency, m is the chargeability, c is the Cole–Cole exponent, and τ is the time constant. Note that this model is only valid for spectral IP data with a singular peak frequency. The present study did observe, however, some IP data that included two peaks. Such data were analyzed by the multi-Cole–Cole model, which introduces the additional terms m_2, c_2, and τ_2 (Pelton et al. 1978; see Appendix 1). The above IP parameters were estimated by an inversion process based on a simulated annealing (SA) technique (Appendix 2).

Results

Resistivity and IP features

Figure 3 shows the depth profiles of resistivity at 1 Hz and phases with frequencies of 0.1 Hz–10 kHz for each site. The figures also compare the resistivity profiles to porosity, and clay and sulfide mineral contents; porosity was estimated based on the water evaporation method, and clay and sulfide mineral contents were determined by X-ray diffraction (XRD) analyses (Appendix 3). Note that the present study defines the sulfide mineral content as the total sum of identified sulfide minerals without sphalerite; this is because sphalerite generally exhibits less electrical conductivity and weaker IP signatures
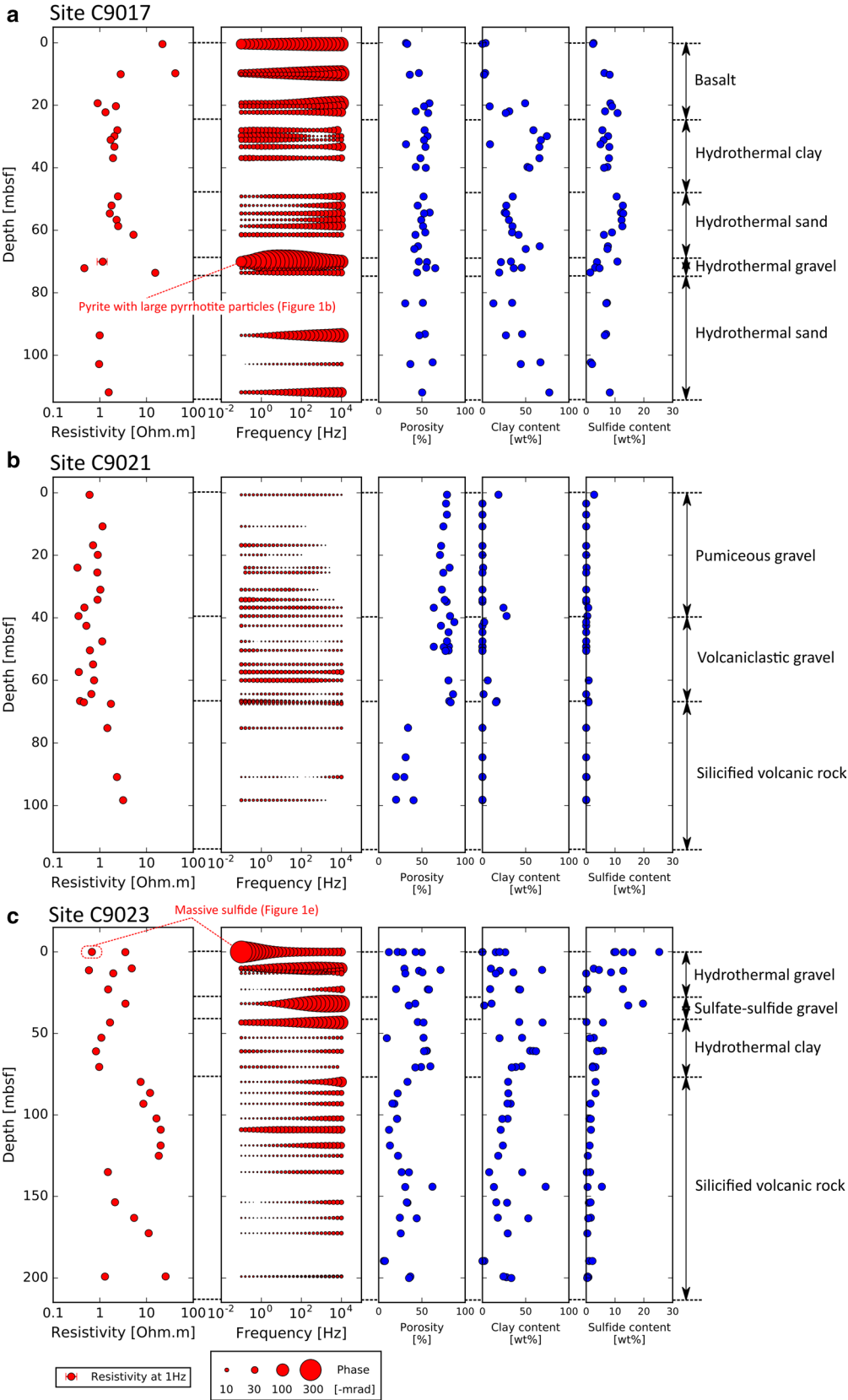
than other sulfide minerals (e.g., Shuey 1975). Resistivity appears to be negatively correlated with porosity. For instance, the resistivity of the hydrothermal sediments from site C9017, with an intermediate porosity of approximately 50%, has values of 1–2 Ωm, while the porous pumiceous gravel from site C9021 (approximately 80% porosity) has a lower resistivity of 0.3–1 Ωm. This negative correlation can also be clearly observed between the resistivity and porosity profiles from site C9023.
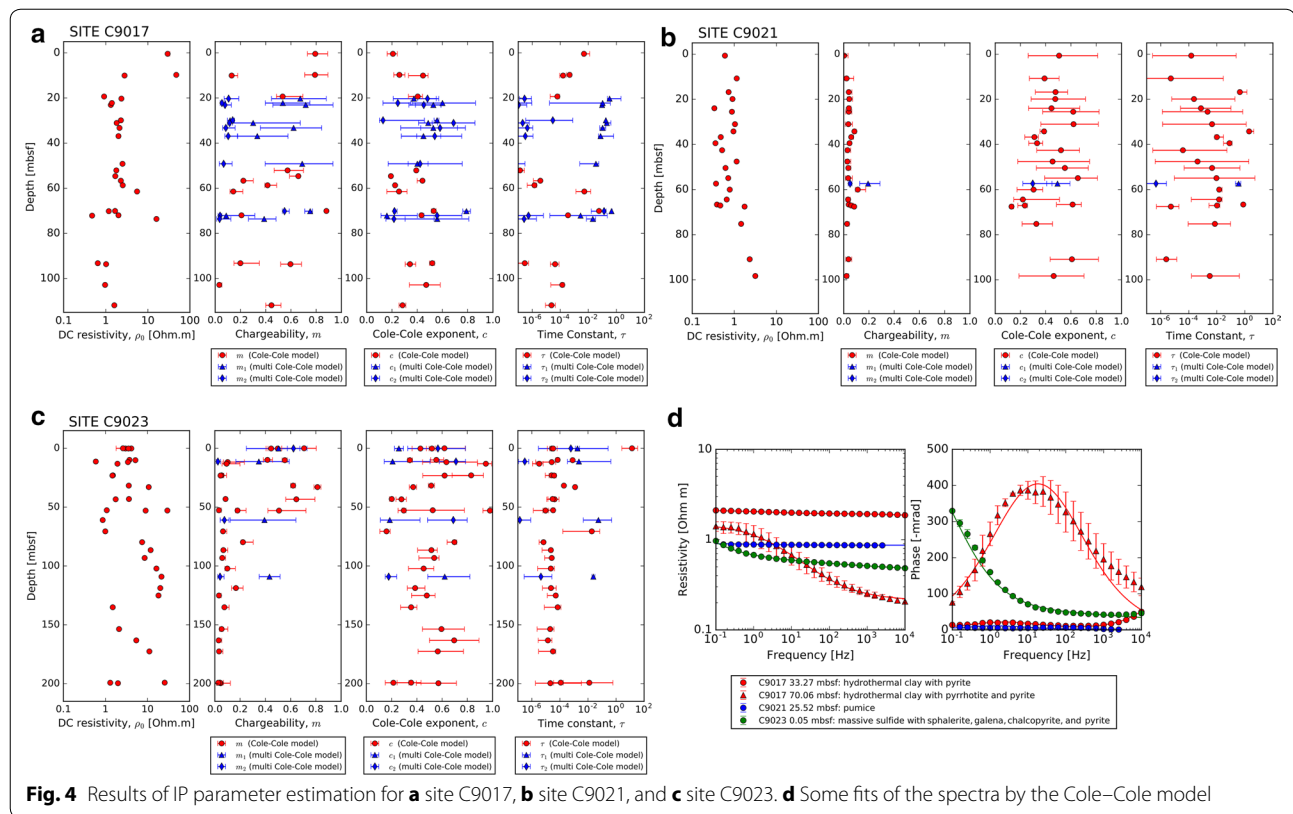
The IP effect is sensitive to the presence or absence of sulfide minerals. Sulfide-poor pumiceous sediments from site C9021 have quite low phases, less than 20 mrad over the whole frequency range. In contrast, the sulfide-bearing hydrothermal sediments from sites C9017 and C9023 exhibit relatively high phase values. A typical feature of the IP effect is that the phase value increases from approximately 10 mrad up to a few hundred mrad with an increase in frequency from 0.1 Hz to 10 kHz. There are, however, three notable exceptions. The 70 mbsf-deep layer at site C9017 where coarse-grained pyrrhotite was observed has a phase peak of 380 mrad at 10 Hz (also see Fig. 4d); this peak frequency is significantly lower than the typical peak frequency of approximately 10 kHz and is higher than any other samples at 10 Hz in the present study. In particular, the subsurface massive sulfide rock obtained from the depth of approximately 0 mbsf at site C9023 has a distinctive spectral IP signature where the phase steadily increases with decreasing frequency, as shown in Fig. 3c. The hydrothermal altered clays at 25–40 mbsf from site C9017 possess two peak frequencies.

(See figure on next page.)
Fig. 3 Results of resistivity and IP measurements, compared with porosity, clay content, and sulfide content, for **a** site C9017, **b** site C9021, and **c** site C9023. Note that sulfide content is defined as the total sum of identified sulfides without less-conductive sphalerite

Komori *et al. Earth, Planets and Space* (2017) 69:114

Page 5 of 10

a Site C9017

Pyrite with large pyrrhotite particles (Figure 1b)

Basalt

Hydrothermal clay

Hydrothermal sand

Hydrothermal gravel

Hydrothermal sand

b Site C9021

Pumiceous gravel

Volcaniclastic gravel

Silicified volcanic rock

c Site C9023

Massive sulfide (Figure 1e)

Hydrothermal gravel

Sulfate-sulfide gravel

Hydrothermal clay

Silicified volcanic rock

Resistivity [Ohm.m]

Frequency [Hz]

Porosity [%]

Clay content [wt%]

Sulfide content [wt%]

Depth [mbsf]

Resistivity at 1Hz

Phase

10 30 100 300 [-mrad]

Komori *et al. Earth, Planets and Space* (2017) 69:114

Page 6 of 10

Fig. 4 Results of IP parameter estimation for **a** site C9017, **b** site C9021, and **c** site C9023. **d** Some fits of the spectra by the Cole–Cole model

Chargeability *m* in IP parameters

Recent significant progress in IP studies has shown that the Cole–Cole exponent "*c*," the time constant "*τ*," and the chargeability "*m*" are essentially functions of the grain-size distribution, the mean radius of sulfide particles, and the volumetric content of sulfide minerals, respectively (e.g., Wong 1979; Dias 2000; Revil et al. 2015a). The present study focuses on the features of *m*, because understanding sulfide abundance and its mineralization is one of the major research objectives of the cruise on which the data were collected.

Figure 4 shows the results of IP parameter estimation, together with some fitting of the spectra to the Cole–Cole model (Fig. 4d). When focusing on chargeability *m*, the pyrrhotite-bearing sediment with high phases up to approximately 400 mrad (70 mbsf, site C9017) exhibits a high chargeability of approximately 0.8. In contrast, low chargeability is estimated for pumiceous sediments with low phases (i.e., less than a few tens of mrad from site C9021). Estimated chargeability and sulfide mineral content are clearly correlated with each other. For instance, the depth profile of chargeability in the core from site C9023, exhibiting a gradual decrease with depth, corresponds well to the transition from the upper sulfide mineral-bearing layer to the lower silicified rocks with lesser amounts of sulfide.

Discussion

In general, resistivity is controlled by the combined factors of connectivity of fluids (a function of porosity), fluid properties (salinity, temperature), surface conductivity of clay minerals, and capacitive behavior due to the presence of clay minerals and sulfide particles (Wong 1979; Revil et al. 1998, 2015a; Zisser et al. 2010). In order to characterize the resistivity and IP properties of the study area, we examined the contribution of these factors to resistivity and IP properties, the factors causing low-resistivity anomalies, and the applicability of IP exploration techniques to submarine hydrothermal deposits.

Features of resistivity (1 Hz) and total chargeability

Figure 5 shows resistivity at 1 Hz and total chargeability as functions of clay and sulfide mineral content, and porosity. Note that total chargeability corresponds to *m* according to Eq. (1) for the single Cole–Cole model. For the multi-Cole–Cole model, chargeability is obtained from the combined contribution of m_1 and m_2 (Pelton et al. 1978). There seems to be no significant correlation between resistivity and sulfide content (Fig. 5b). In contrast, total chargeability is positively correlated with sulfide content (Fig. 5e). The relationship among resistivity, chargeability, and sulfide mineral content is similar to that recently described for disseminated sulfide samples

Komori *et al. Earth, Planets and Space* (2017) 69:114

Page 7 of 10
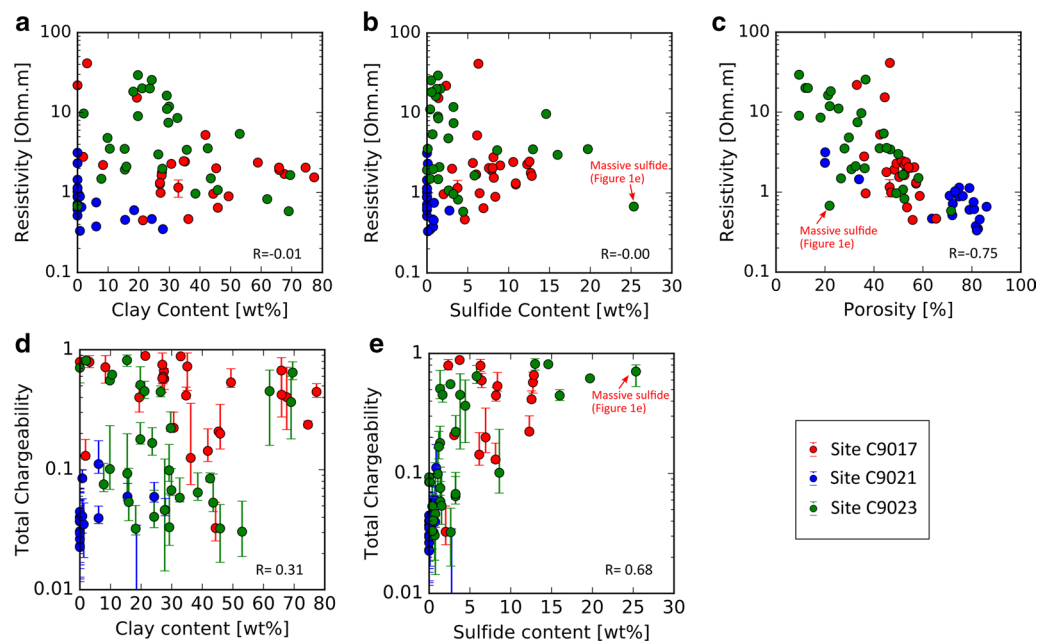
Fig. 5 a–c Comparison between resistivity, clay content, sulfide content, and porosity. **d–e** Comparison between total chargeability, clay content, and sulfide content. The *R* value represents the correlation coefficient

by Revil et al. (2015b). The disseminated sulfide-like characteristics of resistivity and IP properties in the present study are consistent with the visual core description of the drillcore samples including minor amounts of massive sulfide rock.

It is notable that the apparent weak correlation between total chargeability and clay content (Fig. 5d) is considered to be due to the amount of sulfide minerals contained in clay-rich sediments. It is also worth noting that the estimated total chargeabilities are already high values even with small sulfide contents of several wt%. An inhomogeneous distribution of sulfide particles near electrodes might result in an unexpectedly high IP anomaly because of the high sensitivity to data near the electrodes.

Factors controlling resistivity

In the present study, chemical analysis shows that the pore fluid is near-neutral pH and has high salinity similar to typical seawater (Kumagai et al. in prep.); this could cause enhanced electrical conductivity. Further, surface conductivity of clay minerals should also contribute to decreasing bulk resistivity even under high-salinity conditions, because of their high cation exchange capacity (CEC), except for kaolinite (Revil et al. 1998). Hydrothermal clay is predominantly composed of illite, chlorite, and kaolinite in the present study, whereas smectite is found in some samples obtained from depths of 20–50 mbsf at site C9017, and from depths

of 60–67 mbsf at site C9021. Nevertheless, as shown in Fig. 5a, c, resistivity is more sensitive to porosity change than to clay content. This suggests that connectivity of pore fluids primarily controls bulk resistivity in the study area and that clay mineral is a secondary factor affecting resistivity change.

As mentioned previously, resistivity does not correlate with sulfide concentration in terms of the correlation coefficient (Fig. 5c). When focusing on data with sulfide content greater than 5 wt%, resistivity seems to increase with an increase in sulfide concentration. This might correspond to an increase in insulating sulfide at a low frequency such as 1 Hz; this is because fine-grained sulfide particles have high critical frequency for the IP effect (Revil et al. 2015a, b). In contrast, the massive sulfide rock exhibits relatively low resistivity despite its low porosity and high sulfide concentration (Fig. 5b, c), which could be explained by large sulfide particles with the rather low critical frequencies (Fig. 4d). These facts suggest that both the presence of fluids and massive sulfide bodies play an important role in decreasing resistivity when conducting ordinary DC resistivity surveys (i.e., those using a duty cycle with one second current on and off).

High temperature: a possible additional factor in decreased resistivity

In a deep-sea submarine hydrothermal system such as that found at the study site, high temperatures reaching

Komori *et al. Earth, Planets and Space* (2017) 69:114

Page 8 of 10

approximately 350 °C can easily decrease the resistivity of saline fluids up to approximately two orders of magnitude compared to room temperature (e.g., Ussher et al. 2000). Therefore, in active modern submarine hydrothermal deposits, EM and DC resistivity surveys could detect not only massive sulfide bodies, rich in metallic and sulfidic materials, but also high-temperature fluid reservoirs, as low-resistivity anomalies. Notably, the maximum temperature of hydrothermal fluid recorded by ROV observations at Iheya North Knoll is 311 °C (Kawagucci et al. 2013). In particular, at sites C9017 and C9023, relatively small resistivities were obtained by logging while drilling (LWD); these resistivities are up to one order of magnitude smaller than those measured from the drillcore at room temperature (Kumagai et al. in prep.). At both sites, the drill hole discharged high-temperature hydrothermal fluids after drilling, suggesting that in situ high-temperature fluids could be related to the low resistivity values obtained by LWD. Consequently, special care should be taken when interpreting a resistivity structure for the purposes of exploration and exploitation of submarine hydrothermal deposits.

Features of phase peaks

It is well known that the frequency of phase peak depends on the size of sulfide particles and that larger particles cause a phase shift to lower frequencies (Dias 2000; Revil et al. 2015a, b). In the present study, as shown in Fig. 3 and described in the results, the spectral IP property includes two conflicting features: The majority of the samples have phase peaks at high frequencies, although low frequencies were measured in a few samples. For instance, the former and the latter correspond to the samples bearing fine-grained pyrite and those containing relatively coarse-grained pyrrhotite with a radius of approximately 1 mm (found at 70 mbsf at site C9017), respectively. Therefore, the different features of the phase peak appear to be qualitatively explained by the size of the sulfide particles. Likewise, the phase peak with low frequency below 0.1 Hz for the massive sulfide sample (Fig. 4d) could be explained by the presence of the very coarse sulfide mineral.

In addition, the hydrothermally altered clay layer from 25 to 35 mbsf at site C9017 shows two-phase peaks with low and high frequencies, suggesting a bimodal size distribution of sulfide particles, as shown in Fig. 3a. However, this clay layer contains fine-grained pyrite, and no large sulfide particles were observed in visual core description. Instead, this layer includes patchy mottled textures rich in fine-grained sulfide minerals (Fig. 1f); these textures might produce the same spectral IP signature as large sulfide grains.

Applicability of the IP techniques to submarine hydrothermal systems

In the present study, the IP property measurements show that total chargeability is quite sensitive to sulfide mineral content (Fig. 5e), suggesting that IP surveys in submarine hydrothermal systems could detect sulfide-rich bodies as effectively as land-based IP surveys can. In particular, the distinctive IP property of the massive sulfide rock in this study (Fig. 3c) is similar to that observed in terrestrial massive kuroko ore samples of volcanogenic massive sulfide deposits by Yoshikawa and Yoshikawa (1978), who performed time-domain IP measurements and found that the interfaces behave as a kind of Warburg impedance. According to this IP property, they proposed that a long-term injection of current could be effective in identifying massive sulfide bodies on land. Therefore, this methodology would also be effective in seabed surveys.

Notably, high temperatures could also modify spectral IP properties (Zisser et al. 2010), so that IP parameters m, c, and τ depend on temperature. Further investigations in terms of IP dependence on temperature may be needed to examine the robustness of using IP parameters for detection of sulfides in high-temperature hydrothermal systems.

Conclusions and future prospects

The present study successfully determined the depth profiles of resistivity and spectral IP properties of strata composing modern active submarine hydrothermal deposits and identified their primary controlling factors. These outcomes are a valuable guide for a precise interpretation of resistivity structures from marine electromagnetic surveys and provide a constraint on ore-formation models by combining geochemical and mineralogical evidence. Further investigations using drillcore samples will examine the contributions to spectral IP signatures of the species and particle size distribution of sulfide minerals, and the effects of high-temperature environments. It is expected that the progressive accumulation of knowledge about submarine hydrothermal deposits will play an important role in decreasing the risk and cost of exploration and exploitation of these submarine deposits.

Author details
[1] Geological Survey of Japan (GSJ), AIST, Central 7, Higashi 1-1-1, Tsukuba, Ibaraki, Japan. [2] Japan Agency for Marine-Earth Science and Technology (JAMSTEC), 2-15, Natsushima-cho, Yokosuka, Kanagawa, Japan. [3] Kochi Core Center (KCC), Japan Agency for Marine-Earth Science and Technology (JAMSTEC), 200, Mononobe-otsu, Nankoku, Kochi, Japan. [4] Graduate School

Komori *et al. Earth, Planets and Space* (2017) 69:114

Page 9 of 10

of Engineering, Kyoto University, C1-2, Kyoto daigaku-katsura, Nishikyo, Kyoto, Japan. [5] Graduate School of Integrated Sciences for Global Society, Kyushu University, 744, Motooka, Nishi, Fukuoka, Fukuoka, Japan. [6] Japan Agency for Marine-Earth Science and Technology (JAMSTEC), 3173-25, Showa-machi, Kanazawa, Yokohama, Kanagawa, Japan. [7] Graduate School of Science, Kyushu University, 744, Motooka, Nishi, Fukuoka, Fukuoka, Japan. [8] Marine Works Japan LTD., 3-54-1, Higashi, Oppama, Yokosuka, Yokohama, Japan.

are the chargeabilities, c_1 and c_2 are the Cole–Cole exponents, and τ_1 and τ_2 are the time constants.

Appendix 2: Estimation of IP parameters

The present study adopted simulated annealing (SA) to estimate the DC resistivity ρ_0, the chargeability m, the Cole–Cole exponent c, and the time constant τ. This method has the advantage that estimated results depend little on initial conditions, and it is effective in estimating parameters with their uncertainties (e.g., Aarts and Korst 1989). The SA process estimates parameters to fit the calculated spectral IP signatures to observational data. To examine the data fit, the root mean square (rms) error was defined as:

$$\text{rms} = \sqrt{\frac{1}{n_{\text{data}}} \sum_{\omega} \left[\left(\frac{|\rho(\omega)_{\text{data}}| - |\rho(\omega)_{\text{calc}}|}{|e\rho(\omega)_{\text{data}}|} \right)^2 + \left(\frac{\phi(\omega)_{\text{data}} - \phi(\omega)_{\text{calc}}}{|e\phi(\omega)_{\text{data}}|} \right)^2 \right]}, \tag{3}$$

where n_{data} is the total amount of data, $\rho(\omega)_{\text{data}}$ is the observed complex resistivity, $\rho(\omega)_{\text{calc}}$ is the calculated complex resistivity, $e\rho(\omega)_{\text{data}}$ is the observation error of the resistivity, $\phi(\omega)_{\text{data}}$ is the observed phase, $\phi(\omega)_{\text{calc}}$ is the calculated phase, and $e\phi(\omega)_{\text{data}}$ is the observation error of the phase. In the present study, the best-fit model was determined so that the rms error is in the range between 0.95 and 1.05.

Appendix 3: X-ray diffraction analysis (XRD)

In the present study, powdered XRD analyses were performed for quantitative estimation of the mineral composition of rock samples, using the RockJock program (Eberl 2003). High-purity Al_2O_3 (0.25 g; AX-5HM, Hinomoto Kenmazai Co., Ltd., Tokyo, Japan) was used for the internal standard, which was well mixed with 1 g of the powdered sample using 4 ml of ethanol and a shaker. After drying for 10 h at approximately 50 °C, 0.1 g of the mixture was loaded into an XRD glass holder. All scans were run at 45 kV/40 mA with Cu K-α radiation with a divergence slit of 0.25° and a receiving slit of 0.25°, using the X'Pert PRO MPD X-ray diffraction spectroscopy system (Spectris PANalytical, UK).

Appendix 1: Multi-Cole–Cole model

In the case of bimodal distribution of the phase peak frequency, the present study used the multi-Cole–Cole model given as

$$\begin{aligned}\rho(\omega) = \rho_0 &\left[1 - m_1 \left(1 - \frac{1}{1 + (i\omega\tau_1)^{c_1}} \right) \right] \\ &\times \left[1 - m_2 \left(1 - \frac{1}{1 + (i\omega\tau_2)^{c_2}} \right) \right], \end{aligned} \tag{2}$$

where $\rho(\omega)$ is the frequency-dependent complex resistivity, ρ_0 is the DC resistivity, ω is the frequency, m_1 and m_2

Publisher's Note
Springer Nature remains neutral with regard to jurisdictional claims in published maps and institutional affiliations.

Komori *et al. Earth, Planets and Space* (2017) 69:114

Page 10 of 10

References

Aarts E, Korst J (1989) Simulated annealing and Boltzmann machines: a stochastic approach to combinatorial optimization and neural computing. Wiley, New York

Chiba M, Koizumi A, Oshika J, Tanahashi M, Ueda S, Ishikawa N, Okamoto N, Ishizuka O, Shimoda G (2014) Discovery of sulfide mounds in the Okinawa trough. Abstracts with Programs, Soc Resour Geol 64:24 **(abstract)**

Dias CA (2000) Developments in a model to describe low-frequency electrical polarization of rocks. Geophysics 65:437–451. doi:10.1190/1.1444738

Eberl DD (2003) User's guide to RockJock—a program for determining quantitative mineralogy from powder X-ray diffraction data: U.S. Geological Survey Open-File Report 2003-78, 47 p

Kasaya T, Machiyama H, Kitada K, Nakamura K (2015) Trial exploration for hydrothermal activity using acoustic measurements at the North Iheya Knoll. Geochem J 49:597–602. doi:10.2343/geochemj.2.0389

Kawagucci S, Miyazaki J, Nakajima R, Nozaki T, Takaya Y, Kato Y, Shibuya T, Konno U, Nakaguchi Y, Hatada K, Hirayama H, Fujikura K, Furushima Y, Yamamoto H, Watsuji T, Ishibashi J, Takai K (2013) Post-drilling changes in fluid discharge, mineral deposition patterns and fluid chemistry for the seafloor hydrothermal activity in the Iheya-North hydrothermal field, Okinawa Trough. Geochem Geophys Geosyst 14:4774–4990. doi:10.1002/ggge.20283

Kowalczyk P (2008) Geophysical prelude to first exploitation of submarine massive sulphides. First Break 26:99–106

Kumagai H, Nozaki T, Ishibashi J, Maeda L, CK16-01 on-board member (in preparation) Cruise report SIP -HOT II "Explorer" (SIP-Hydrothermal deposit in Okinawa Trough) CK16-01 (Exp. 908), JAMSTEC, Yokosuka, Japan

Leroy P, Revil A, Kemna A, Cosenza P, Ghorbani A (2008) Complex conductivity of water-saturated packs of glass beads. J Colloid Interface Sci 321:103–117. doi:10.1016/j.jcis.2007.12.031

Okada C, Kubota R, Ishikawa H, Iwamoto H, Kanai Y, Takahashi M, Matsuda T, Kasaya T (2017) Preliminary report of self-potential and resistivity explorations in the Izena Hole. In: Proceedings of the 136th SEGJ conference, Tokyo, Japan

Pelton WH (1977) Interpretation of complex resistivity and dielectric data. Dissertation, University of Utah

Pelton WH, Ward SH, Hallof PG, Sill WR, Nelson PH (1978) Mineral discrimination and removal of inductive coupling with multifrequency IP. Geophysics 43:588–609. doi:10.1190/1.1440839

Revil A, Cathles LM III, Losh S, Nunn JA (1998) Electrical conductivity in shaly sands with geophysical applications. J Geophys Res 103(B10):23925–23936. doi:10.1029/98JB02125

Revil A, Florsch N, Mao D (2015a) Induced polarization response of porous media with metallic particles—part 1: a theory for disseminated semiconductors. Geophysics 80:D525–D538. doi:10.1190/geo2014-0577.1

Revil A, Aal GZA, Atekwana EA, Mao D, Florsch N (2015b) Induced polarization response of porous media with metallic particles—part 2: comparison with a broad database of experimental data. Geophysics 80:D539–D552. doi:10.1190/geo2014-0578.1

Shuey RT (1975) Semiconducting ore minerals, vol 4. Developments in Economic Geology, Elsevier, Amsterdam

Takai K, Mottl MJ, Nielsen SHH, the IODP Expedition 331 Scientists (2012) IODP Expedition 331: strong and expansive subseafloor hydrothermal activities in the Okinawa Trough. Sci Drill 13:19–27. doi:10.2204/iodp.sd.13.03.2011

Takai K, Kumagai H, Kubo Y, CK1404 on-board member (2015) Cruise report SIP-HOT I "Pathfinder" (SIP-Hydrothermal deposit in Okinawa Trough) CK14-04 (Exp. 907), JAMSTEC, Yokosuka, Japan, p 116

Ussher G, Harvey C, Johnstone R, Anderson E (2000) Understanding resistivities observed in geothermal systems. In: Proceedings World Geothermal Congress 2000, Kyushu-Tohoku, Japan

Wong J (1979) An electrochemical model of the induced-polarization phenomenon in disseminated sulfide ores. Geophysics 44:1245–1265. doi:10.1190/1.1441005

Yoshikawa H, Yoshikawa M (1978) On the I.P. characteristics of Kuroko ore deposits. Min Geol 28:163–175. doi:10.11456/shigenchishitsu1951.28.163

Zisser N, Kemna A, Nover G (2010) Dependence of spectral-induced polarization response of sandstone on temperature and its relevance to permeability estimation. J Geophys Res 115:B09214. doi:10.1029/2010JB007526